Supporting Information

A Reference-Free Traction Force Microscopy Platform Fabricated via Two-Photon Laser Scanning Lithography Enables Facile Measurement of Cell-Generated Forces

*Omar A. Banda, Chandran R. Sabanayagam, John H. Slater**

*Corresponding Author; Email: jhslater@udel.edu

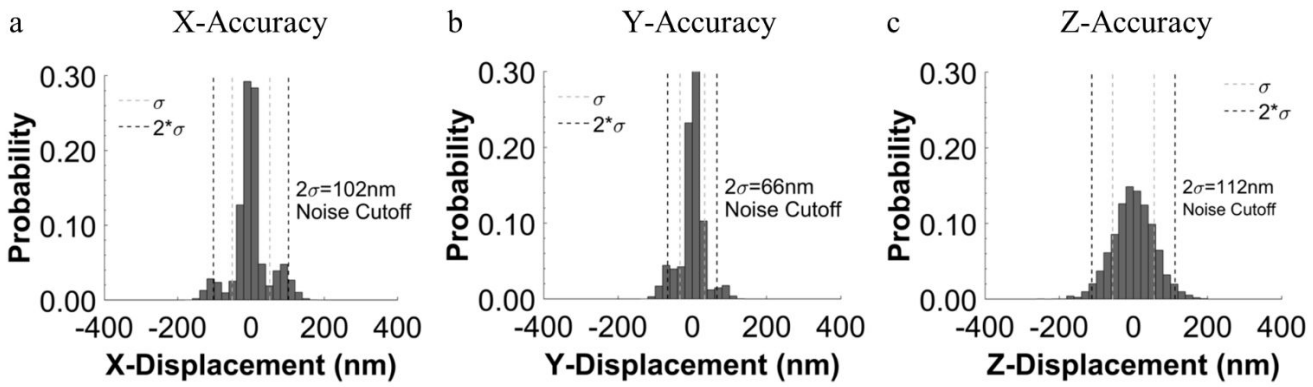

Figure S1. Quantifying the accuracy of the implied reference. (a,b,c) Histograms displaying the accuracy of reference lines for each cardinal direction, shown as the probability of locating marker centroids in a non-stressed array. The darker dashed vertical lines indicate two standard deviations from the mean and this value was used to set the lower limit for displacement measurements. Accuracy in each direction varies due to the different modes of stepping used during patterning. (n = 2,651 markers tracked for each direction). See main manuscript text for average over many volumes.

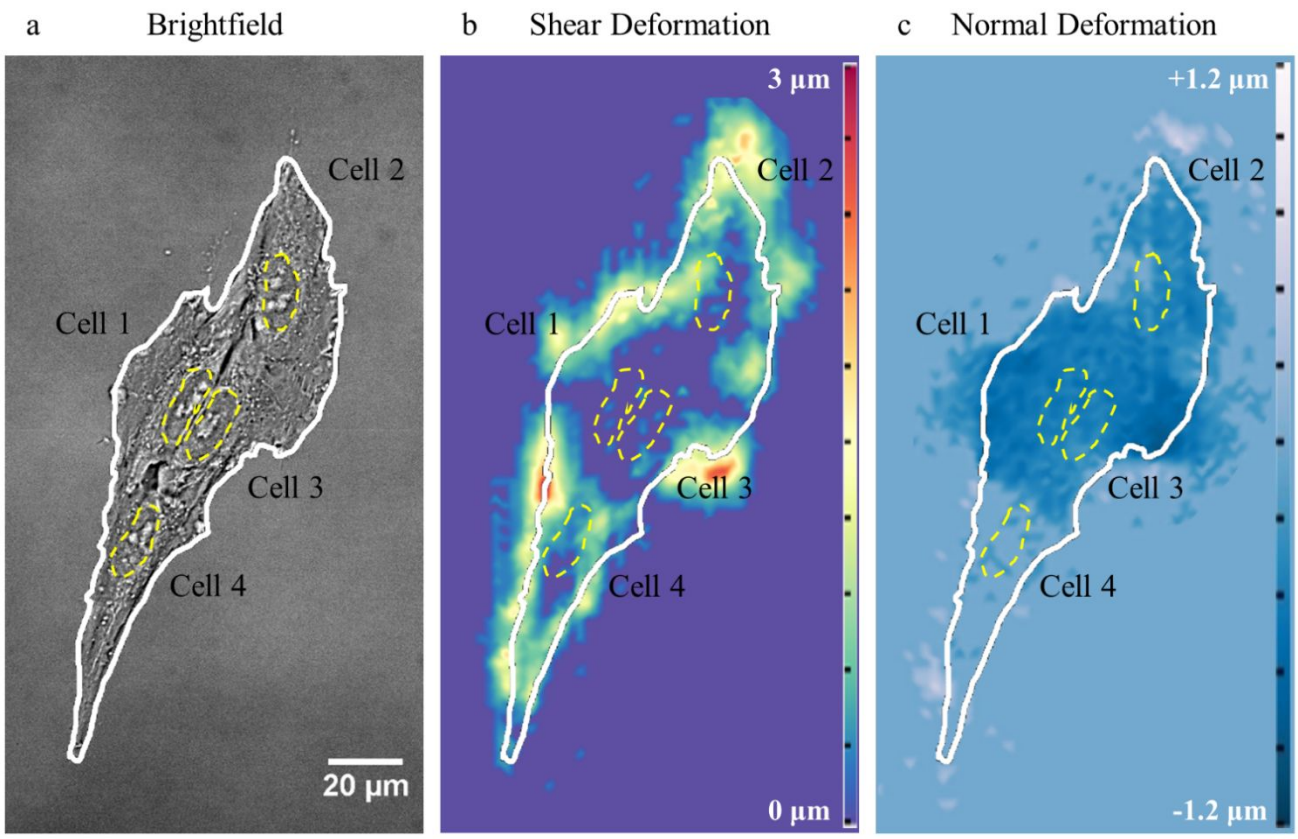

Figure S2. Material deformation induced by a cell cluster. (a) Brightfield image of a cluster of four HUVECs given arbitrary number assignments. The nucleus of each cell is outlined with a dashed yellow line. (b) Shear deformation induced by the cell cluster. (c) Normal deformation induced by the cell cluster. While the spatial distribution of shear and normal deformation in cell clusters does not match individual cells, the ratio of shear to normal still holds. For example, cell number 4 generates minimal normal deformation, despite generating large shear deformation.

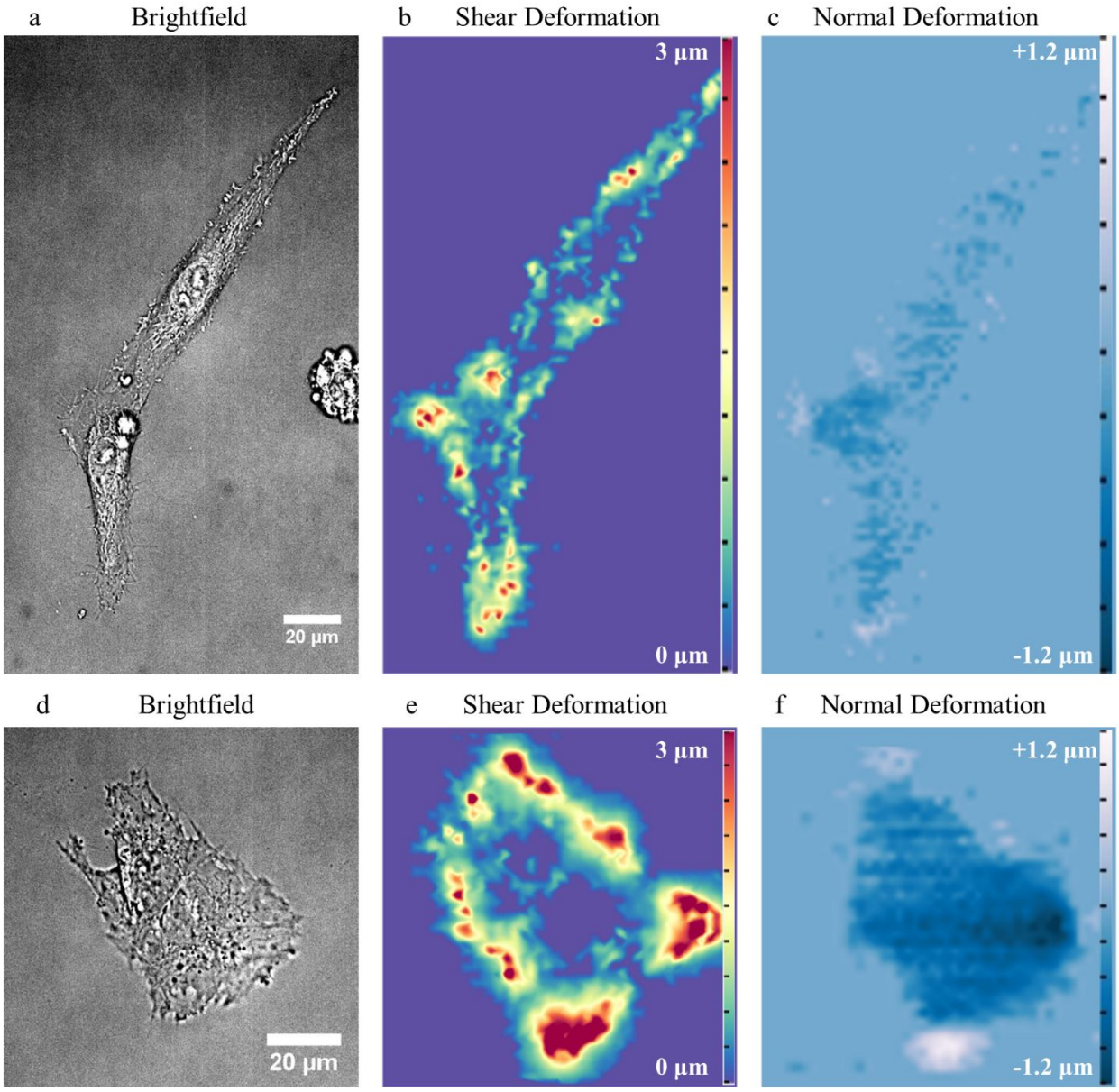

Figure S3. Material deformation induced by cell clusters. (a,d) Brightfield images of clusters of 2 HUVECs. (b,e) Shear deformation induced by the cell clusters. (c,f) Normal deformation induced by the cell clusters.

Video S1. Time-lapse of a spread HUVEC. Shown are (a) transmitted and (b) z-projected fluorescence images of a spread HUVEC captured at 15 min intervals over 90 min. The interpolated displacement fields of (c) shear and (d) normal deformation measured from the fluorescent image stack.

Video S2. Time-lapse of a spreading HUVEC. Shown are (a) transmitted and (b) z-projected fluorescence images of a spread HUVEC captured at 15 min intervals over 90 min. The interpolated displacement fields of (c) shear and (d) normal deformation measured from the fluorescent image stack.

Materials & Methods

All materials were purchased from Sigma-Aldrich (Sigma-Aldrich, St. Louis, MO) unless otherwise specified.

Cell Culture

Human Umbilical Vein Endothelial Cells (HUVECs, Lonza, Catalog No. C2519A) were cultured in EGM-2 media (Clonetics™ EGM™-2 BulletKit™; Lonza Catalog No. CC-3162; 500 ml of EBM™-2 Medium and the following supplements: human Epidermal Growth Factor (hEGF), 0.5 ml; Vascular Endothelial Growth Factor (VEGF), 0.5 ml; R3-Insulin-like Growth Factor-1 (R3-IGF-1), 0.5 ml; Ascorbic Acid, 0.5 ml; Hydrocortisone, 0.2 ml; human Fibroblast Growth Factor-Beta (hFGF-β), 2.0 ml; Heparin (0.5 ml); Fetal Bovine Serum (FBS), 10.0 ml; Gentamicin/Amphotericin-B (GA), 0.5 ml) during expansion and traction force microscopy (TFM) experiments. HUVECs were cultured at 37 °C and 5% CO_2 and the media was changed every two days. HUVECs were passaged at ~80% confluency and cultured on TFM hydrogels at passage 7 for all experiments.

ASC52telo, hTERT immortalized adipose-derived mesenchymal stem cells (ATCC® SCRC-4000™) (ASCs) were cultured in mesenchymal stem cell growth medium (ATCC Catalog No. PCS-500-040, PCS-500-30) containing 482 mL of basal medium, 10mL of MSC supplement (2% FBS, 5 ng/mL rh FGF basic, 5 ng/mL rh FGF acidic, 5 ng/mL rh EGF), 6mL of L-Alanyl-L-Glutamine (2.4mM, final concentration) and 2 mL of 50mg/ml G418 (0.2mg/mL, final concentration), and passaged at ~80% confluency.

Synthesis of PEGDA

PEGDA (3.4kDa) was synthesized as previously described[1,2]. Briefly, poly(ethylene glycol) (3.4kDa; Cat.# 202444-500G) was reacted with acryloyl chloride (AC; Cat.#549797-5G) in the presence of triethylamine (TEA; Cat.#471283-500ML) in anhydrous dichloromethane (DCM; Cat.#270997-100ML) at molar ratios of 4:1 (AC:PEG) and 2:1 (TEA:PEG) overnight under argon. The result was mixed vigorously with an aqueous K_2CO_3 (Cat. #791776) solution and allowed to reach a visible phase-separation over 24 hrs. $MgSO_4$ (Cat. #M7506) was added to the organic phase to remove any remaining aqueous contaminants. The purified organic solution containing PEGDA was distilled through rotary evaporation to remove excess DCM. PEGDA was precipitated from the remaining DCM in cold diethyl ether, isolated through vacuum filtration, and thoroughly dried. The final PEGDA product was analyzed via ^{1}H-NMR to confirm substitution of terminal hydroxyls for acrylates.

Synthesis of Acrylated-PEG Derivatives

To synthesize acrylate-PEG-RGDS, a hetero-bifunctional PEG with a chain-end acrylate and succinimidyl-ester (PEG-SVA; Laysan Bio; Arab, AL; Cat. # ACRL-PEG-SVA-3400-500mg) was reacted with the amine terminus of the peptide sequence RGDS (GenScript; Piscataway, NJ; Cat.# RP10861) in the presence of diisopropylethylamine (Cat.# D125806) in DMSO (Cat.# 276855) for 24 hrs. The product was dialyzed against ultrapure water with 4 exchanges at least 2 hrs apart over 2 days. The aqueous product was frozen at -20 °C for 24 hrs, -80 °C for 4 hrs, and lyophilized for 2 days at -85 °C at 0.120 mbar followed by analysis via gel permeation chromatography in ultrapure water to estimate purity (>90% Acryl-PEG-RGDS). Fluorophore-labeled PEG acrylate was synthesized in a two-step reaction through similar NHS-chemistry. First, diamine-PEG (Laysan Bio; Cat.# NH2-PEG-NH2-2K-1g) and either AlexaFluor488 (AF488), or AlexaFluor633 (AF633) succinimidyl ester (ThermoFisher; Cat.# A20000/A20005) were reacted at a molar ratio of 75:1 in DMSO in the presence of

diisopropylethylamine for 24 hrs. The resulting products were reacted with PEG-SVA (165:1, PEG-SVA:AlexaFluor dye) for 24 hrs. As before, the product was dialyzed and lyophilized. All PEG derivatives were stored at -80 °C under Argon until use.

Base Hydrogel Formulation and Photopolymerization

Base hydrogels were polymerized through a photo-initiated radical polymerization reaction. With sterile PBS (pH 7.4) as a solvent, hydrogel formulations were 5% mass-to-volume PEGDA, 10 mM PEG-RGDS, and were doped with 0.08% mass-to-volume AF488-labeled PEG-derivative to allow for visualization via fluorescence microscopy. The photo-initiator, lithium phenyl-2,4,6-trimethylbenzoylphosphinate (LAP), was synthesized as previously described[3]. Briefly, dimethyl phenylphosphonite was reacted with an equimolar amount of 2,4,6-trimethylbenzoyl chloride under argon for 24 hrs with stirring. A fourfold excess of lithium bromide in 100 ml of 2-butanone was added to the reaction and heated to 50 °C for 10 mins. The solution was cooled to room temperature over 4 hrs, vacuum filtered, and washed with 300 ml of 2-butanone. The product was dried in a fume hood, stored in an amber vial at 4 °C, and used at a concentration of 3 mg/ml. The hydrogels were photopolymerized under a broad spectrum UV lamp (UVP; Blak-Ray™ Model B-100AP/R lamp; ~12 mW at 370 nm) for 1 min between a thin smooth sheet of perfluoroalkoxy alkanes (PFA, McMaster Carr) and an methacrylate-silane functionalized glass coverslip. The coverslip-bound hydrogel was stored in sterile buffer.

Nano-Indentation Testing of Patterned and Non-Patterned Hydrogels

Operating under the assumption that PEGDA hydrogels are linear elastic materials, nanoindentation experiments were performed on the surface of the hydrogels in patterned and non-patterned areas. All indentations were performed using a Bruker BioScope Catalyst BioAFM indenter with a custom tip

comprising a 0.6 N m^{-1} Silicon Nitride cantilever and 45 μm diameter polystyrene spherical end. Indentation was performed at a rate of 2 μm s^{-1} to a trigger threshold of 72 nN. Force-indentation curves were collected for patterned (n=66 total curves from 3 regions) and non-patterned (n=63 curves from 3 regions) regions, and Young's modulus was approximated from fits of the retraction with force boundaries of 10-70% of the maximum using a spherical Hertzian model. All fits were performed in the NanoScope Analysis software package (v1.5).

Two-Photon Laser-Scanning Lithography for Fiducial Marker Patterning

A base hydrogel was assembled into a fluidic chamber (**Figure 1**) within a custom-designed and machined stage insert fitting the motorized stage on an upright Zeiss LSM 780 confocal microscope. A soaking solution (containing 5% mass/volume of the acryl-PEG-AF633, 1% volume/volume N-Vinylpyrrolidone, and 3 mg/ml LAP) was flowed into the soaking chamber containing the base hydrogel. An argon laser line (488nm) identified the AF488 signal in the base gel and was used to navigate to the center and surface of the hydrogel. Using a series of XZ tile scans, the surface of the hydrogel was leveled using set screws in the custom-built stage insert to improve spatial consistency of the pattern array relative to the surface. A Chameleon Vision 2 (Coherent Inc.; Santa Clara, CA) tuned to 740nm operating at a fluence of 3.7 nJ/μm^2 focused through a Zeiss C-Apochromat 40X 1.2 NA water-immersion objective was scanned at desired locations in the base hydrogel to initiate photo-polymerization of the fluorescently-labeled PEG monoacrylate. A digital mask containing single pixel features (~9.4 pixels/micron) was used to guide the position of the laser to specify pattern locations. The patterning scheme used contained a single row of 100 single pixel features with designated object spacing of 2.12 μm in the X-direction. Spacing in the Y- and Z-directions were controlled using the tile and z-stack functions respectively, in Zen software, and were specified as 2.12 μm in Y and 3.5 μm in Z. Patterning parameters were adjusted to reach a patterning speed of 1.25 mm^2 per hour. The resulting fiducial markers

resembled 3D Gaussian-like features with full-width, half-max dimensions of 0.84 ± 0.108 μm in XY and 3.73 ± 0.304 μm in Z.

Two-Photon Laser-Scanning Lithography for Patterning Adhesive Ligands

To incorporate the cell adhesive peptide, RGDS, a base hydrogel which did not contain acrylate PEG-RGDS was synthesized and patterned as described above. To add RGDS to the surface, PEG-RGDS was dissolved at a 10 mM concentration in the solution used for creating fiducial markers. This solution was soaked into the base hydrogel already decorated with fiducial markers. The hydrogel was allowed to reach a stable swelling point, and then TP-LSL was implemented using the same laser settings for creating fiducial markers to generate fluorescent adhesive regions.

Imaging Material Deformation During Cell Experiments

Before use, patterned hydrogels were rinsed in sterile PBS over 2 days with 4 exchanges of the sterile PBS wash solution. All fluorescent images of patterned features were captured using a Zeiss C-Apochromat 40X 1.2 NA water-immersion objective on a Zeiss AxioObserver Z1 microscope equipped with the Apotome2 structured illumination module and ORCA-Flash 4.0LT camera (Hamamatsu) with a 162.5 nm pixel size. Z-stacks were acquired at 0.4 μm intervals. Confocal quality images using the structured illumination were achieved using 3 phase images per captured view field. HUVECs or ASCs were seeded on patterned hydrogels at a density of ~ 40 cells/mm^2 in EGM-2 or MSC growth media, respectively. HUVECs were given at least 2 hrs to adhere before imaging. Time-lapse imaging was performed on the same Zeiss AxioObserver Z1 using a temperature-controlled enclosure set to 37 °C and 5% CO_2 with the sample on a heated stage insert set to 37 °C. Time-lapse brightfield and fluorescent images were acquired every 15 mins for 90 mins.

Measuring Cell-Induced Material Displacements

The following processing and analytical methods were performed using custom code written in Matlab, which may be accessed in an online public repository[4].

Image Processing: To reduce computational time in later steps, raw image stacks were cropped to regions containing a single cell or cell cluster and sufficient surrounding space to include non-stressed reference locations. Cropped image stacks of fluorescent markers were processed using a custom MatLab script (bpass3dMB.m; Maria Kilfoil 2005, based on Crocker and Grier 1991.[5–7]) which performs a 'mexican hat' wavelet convolution independently on all image axes using a one-dimensional kernel described by the vector:

$$\left[\left(\frac{e^{-\left(\frac{-r}{2N}\right)^2}}{S}+\frac{-1}{2r+1}\right),\left(\frac{e^{-\left(\frac{-r+1}{2N}\right)^2}}{S}+\frac{-1}{2r+1}\right),\ldots,\left(\frac{e^{-\left(\frac{r}{2N}\right)^2}}{S}+\frac{-1}{2r+1}\right)\right]$$

, where $S=\sum_{i=-r}^{r}\left(e^{-\left(\frac{i}{2N}\right)^2}\right)$, r is an integer describing a pixel length slightly larger than the expected radius in the respective dimension of a feature, and N describes the characteristic length scale of noise in the data in that same dimension.

2D Object Detection: Subpixel XY localizations of marker centroids in each plane within a Z-stack were detected using custom Matlab scripts (feature2D.m, localmax.m, rsqd.m, fracshift.m; Maria Kilfoil 2003, based on IDL code by John C. Crocker 1993 and David G. Grier 1992.[5–7]), which are based on finding a local intensity maxima in each 2D image and contains features including a minimum separation distance and a minimum intensity value to qualify as a detection. Subpixel localization is accomplished by approximating a center of mass (intensity) from an interpolated subarray centered around each detection with subarray dimensions related to the approximate expected radius of detections (**Figure S4**).

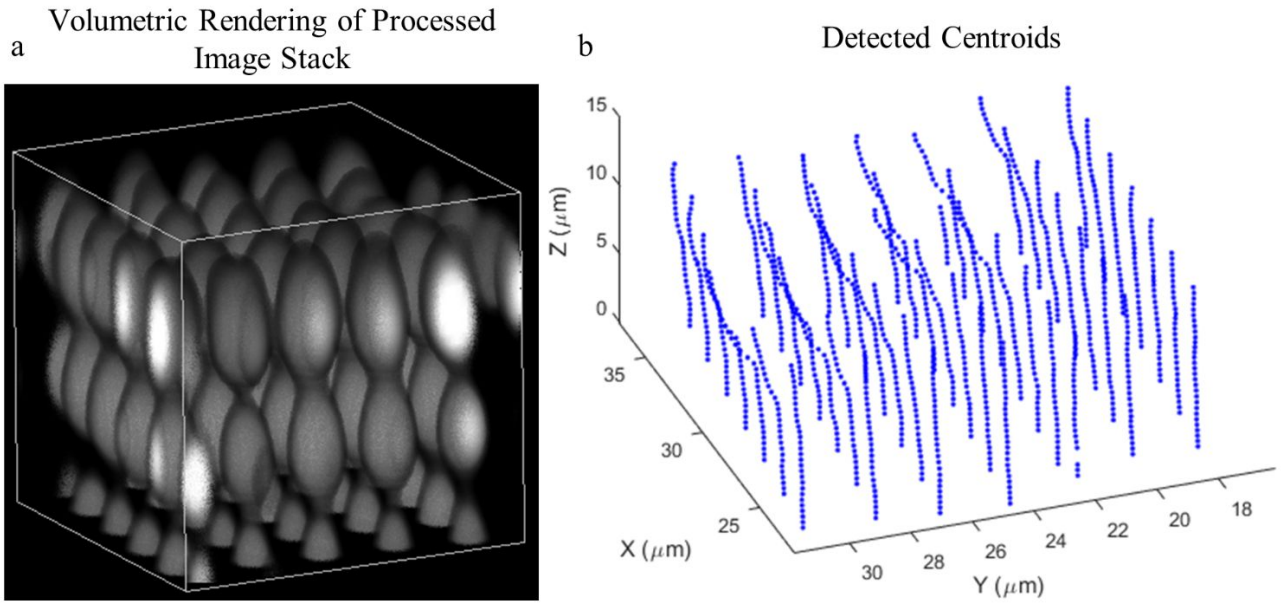

Figure S4. Two-dimensional object detection. (a) A volumetric rendering of a small volume of a processed image stack. (b) A centerline is traced through the long dimension (Z-direction) of the ellipsoids in the volumetric rendering. Detecting centroid locations on the center line, frame by frame in Z, is the first step in measuring deformation.

2D Object Linking through the Z-Dimension (Columns): Before measuring fluorescent marker shear displacement, detected objects were linked through the Z-dimension using custom particle tracking Matlab scripts (trackmem.m[7]) (**Figure S5**). The algorithm groups objects frame-by-frame through an overall minimization of object displacements. Errors in grouping were manually corrected using a custom Matlab script coding for an interactive user interface that provides the user with traces of grouped objects overlaying a Z-projection image as a visual-aid. Errors in automatic linking typically occurred in locations of large deformations and were relatively few (<< 1%)**.**

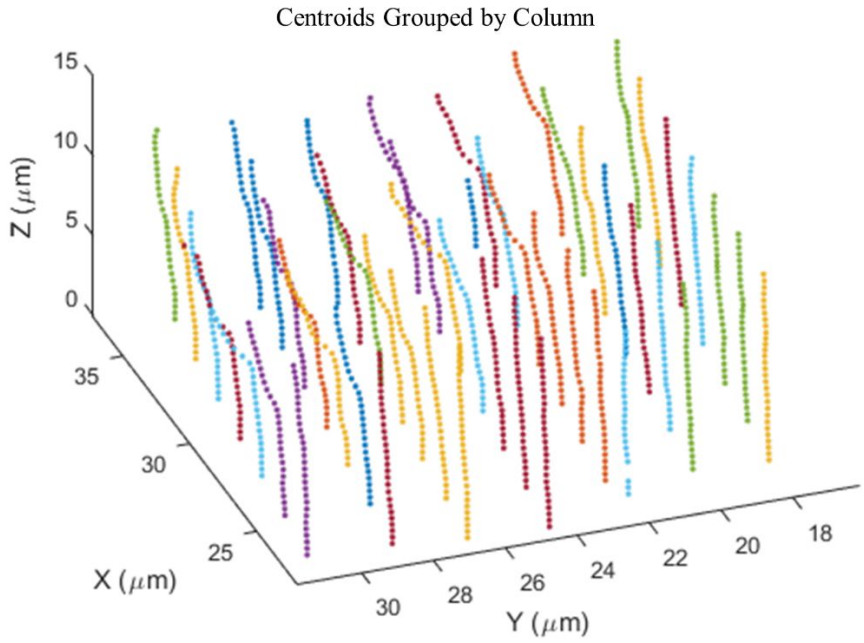

Figure S5. Linking detected centroids through the Z-direction. Detected centroids are grouped into columns using particle tracking analysis.

Approximating XY Reference Locations to Measure Shear Deformation: The assumption required for making measures of deformation in the XY plane was that detections which are sufficiently below the surface of the hydrogel were representative of the XY positions of non-deformed detections near the surface (**Figure S6a**). This assumption held true for the vast majority of cases after reaching depths of ~10-12 μm from the hydrogel surface (it should be noted that at this depth, deformations normal to the surface can often still be detected). The orientation of the 3D arrays within the hydrogels were not always perfectly level with the surface. This was accounted for by the inclusion of an algorithm to predict the contribution of tilt to the measured displacements as a function of depth, and the predicted contribution was subtracted from final displacement measures (Figure S6b). Briefly, for each displacement measure, the algorithm searched for the nearest non-deformed columns of detections. The average linear fit of the

non-deformed columns was used to determine the appropriate correction factor for each measure of displacement based on its depth.

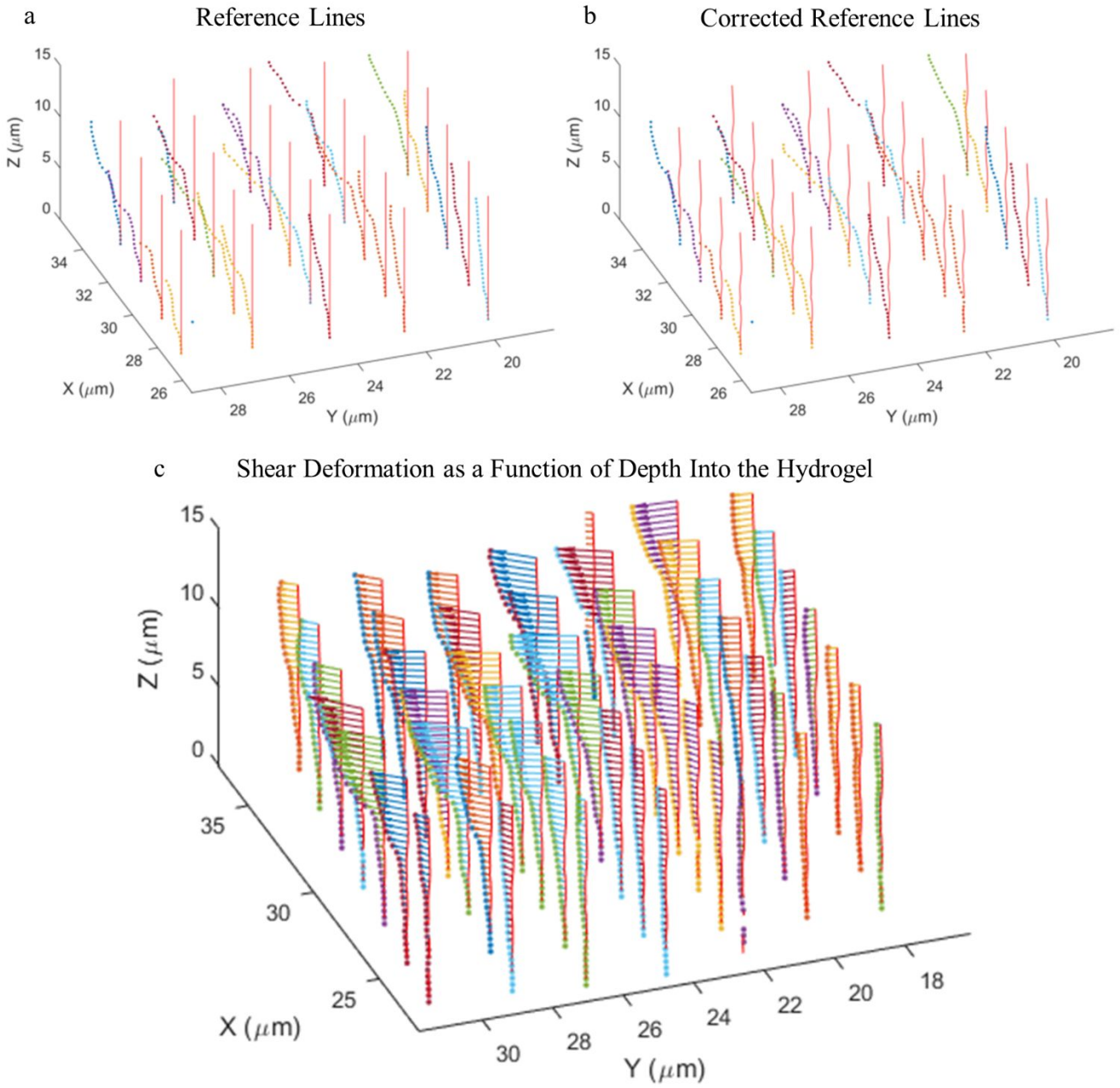

Figure S6. Determining the reference state and measuring shear deformation. (a) Initial XY reference coordinates are determined from the XY locations of the deepest markers in the array; furthest from the surface of the hydrogel. (b) The reference coordinates are corrected for tilt and others errors that occur in the patterning process, such as shifts in the X-direction in some rows. (c) Shear deformation within the hydrogel is measured as a function of depth from the hydrogel surface.

Object Detection for 3D Displacements: 3D subpixel localization of marker centroids within a Z-stack were detected using custom Matlab scripts (feature3dMB.m, llmx3dMB.m, fracshift3dMB.m, lrsqd3dMB.m; Yongxiang Gao and Maria Kilfoil 2005, based on IDL code by John C. Crocker and David G. Grier 1999.[5–7]), which are based on finding local maxima of intensity in the 3D image stack and include features such as a minimum separation distance between detections and a minimum intensity value to qualify as a detection. Subpixel localization is accomplished by approximating a center of mass (of inten sity) from an interpolated subarray centered around each detection with subarray dimensions related to the approximate expected radius of detections input by the user (**Figure S7**).

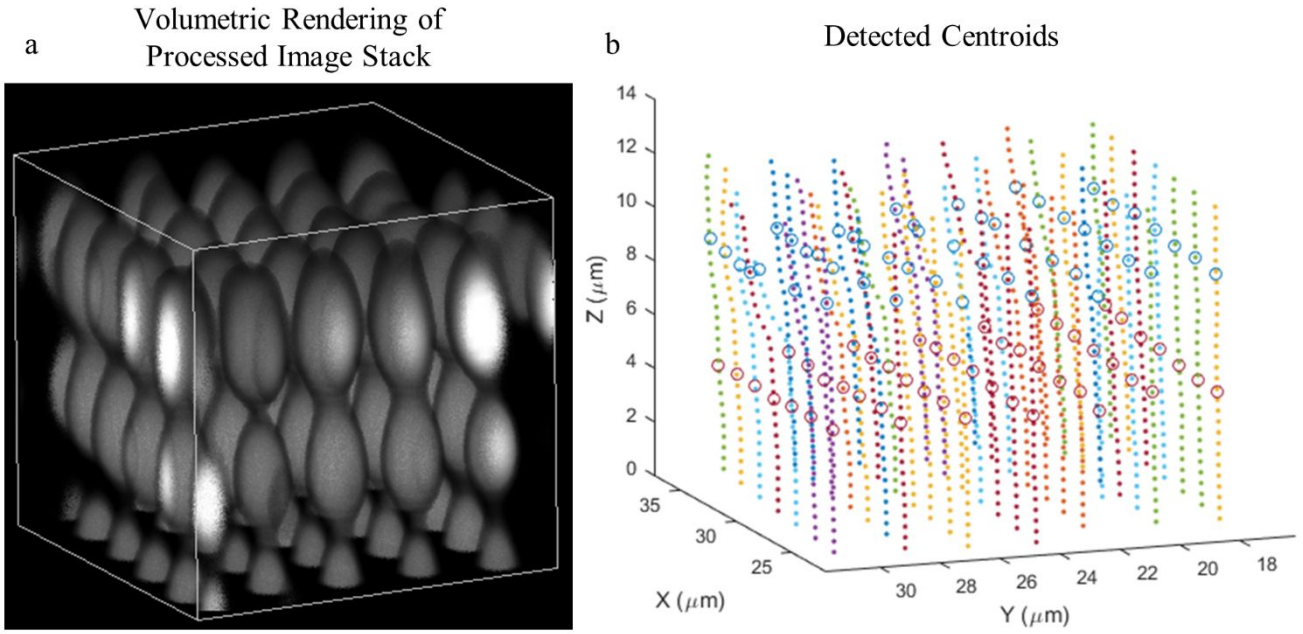

Figure S7. 3D centroid detection. (a) A volumetric rendering of a small volume of a processed image stack. (b) To obtain accurate 3D deformation measurements, the centroids of ellipsoids were detected. Ellipse centroids (circles) are plotted over previous shear detections (dots).

Object Linking through the X-Dimension (Rows): Limitations in the number of single pixel regions that could be loaded in the LSM software forced the feature arrays to be scribed line-by-line, with each line (100 features) being printed several times through the Z-direction before the stage shifted in the X-

direction to the next frame. Y-direction shifts occurred after all Z-planes in each frame through the X-direction at a given Y coordinate were scribed. As an overall result of this process, rows in the X-direction (printed all at once by the scanning galvometers) had better Z-positioning precision than rows in the Y-direction (printed one at a time with an automated stage shift between each). The array's X-dimension was determined algorithmically by identifying which array axis demonstrated a higher Z precision within non-deformed detections. Once determined, a characteristic row vector describing the slope of a non-deformed row was identified. Detections within a given plane were sequentially grouped into rows by starting with the coordinates of a seed detection, adding or subtracting a vector parallel to the row vector with length 2.12 μm, and creating a search window near the new location to find the closest candidate detection to be added to the same row; this process was repeated until no new detections were found for a given row, and then a new seed detection was chosen, and the process was repeated (**Figure S8a**).

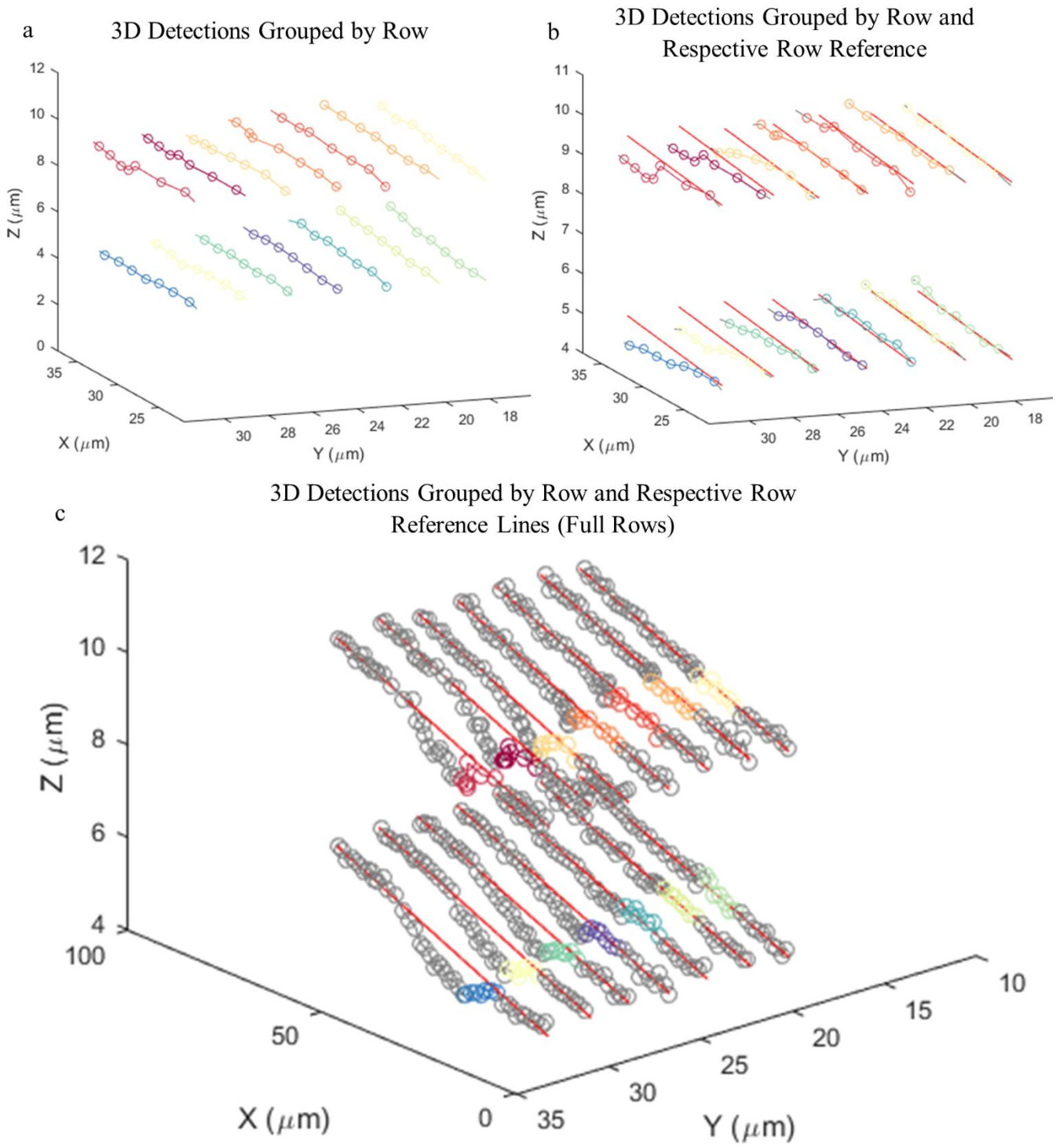

Figure S8. Grouping object detections by row. (a,b) Detections were grouped into rows in the X-direction to generate reference lines. (b) Detections and row traces are plotted in matching colors, and reference lines plotted in red. (c) The full rows, including non-deformed detections, help visualize the quality of row fits.

Approximating Z Reference Locations to Measure Displacement: Detections were grouped based on whether they were likely to be displaced. This distinction was made by digitally dilating a binary mask of a cell boundary by ~ 8μm (which was deemed a sufficient distance from a cell boundary to no longer register deformation), and designating all features occurring outside of the mask as unlikely to be displaced. Detections occurring within the XY coordinate space of the dilated cell boundary were identified and ignored during the linear fits used to determine reference coordinates.

X and Y reference coordinates for 3D detections were determined by identifying which column each detection belonged to and assigning the appropriate corrected XY reference coordinates. For approximating Z reference coordinates, two separate approaches were employed. *Method 1*. The default approach used non-deformed detections within a row to generate a best-fit line assumed to pass through all reference coordinates. From this line, Z reference coordinates were then approximated by finding the closest matching XY coordinates on the fit line to the XY reference coordinates and solving for the Z reference coordinate. This method worked well for rows where displaced features were flanked by non-displaced features in each region of interest, but did not work well in cases where there were too few non-displaced features. *Method 2*. To deal with exceptional cases of the second type, for each plane of detections, an average best-fit line was formulated based on the best-fit lines of rows meeting criteria for Method 1. The average best-fit line was then translated in 3D space to best fit non-displaced detections in rows which were not good candidates for fitting based on method 1, and had at least 1 non-displaced marker.

Once Z reference lines were determined, final 3D reference coordinates were approximated as the intersection between XY and Z reference lines (**Figure S9a**). Fiducial marker displacements were then

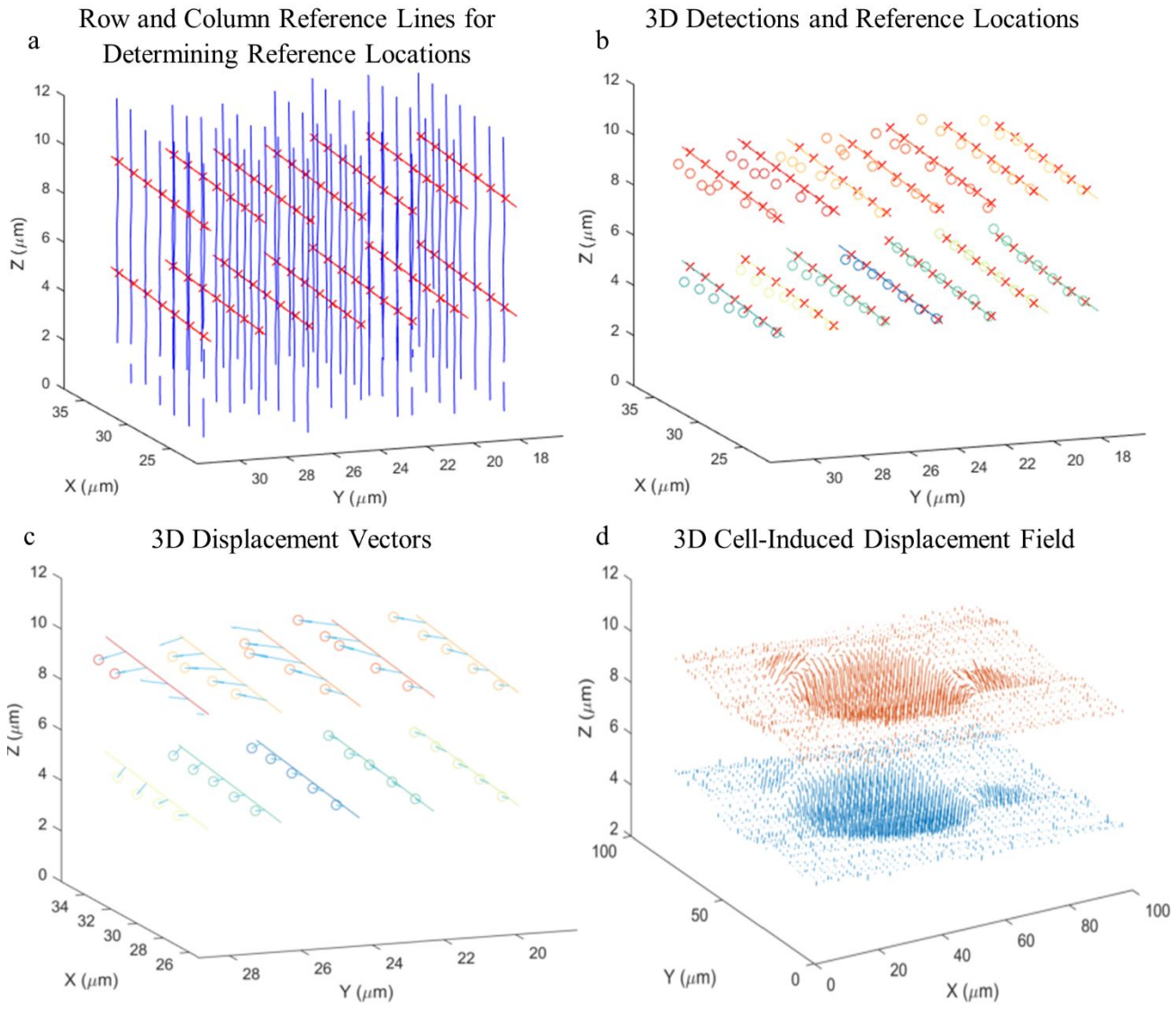

Figure S9. Measuring 3D displacement fields. (a) After grouping by row, 3D detections were also grouped by column based on previously determined reference locations. (b,c) The intersections of these reference lines were used to generate the 3D reference coordinates for each detection to measure 3D displacement. (d) An example displacement data set for a single cell is provided to visualize the overall 3D nature of collected deformation profiles.

calculated as the difference between these reference coordinates and fiducial marker centroids (Figure S9b-d).

Relating Shear and Normal Displacement Distributions

Line profiles of shear and normal displacements were created to visualize the spatial relationship between shear and normal components of tractions induced by HUVECs. The centroid of a binarized image of each cell's spread area was approximated based on a center of mass calculation. A line was traced from the centroid of the cell through the XY coordinates of the point of maximum shear displacement for each cell to create a displacement profile, averaged over a width of 3.25 μm in the XY plane about the trace. For each case, the shear displacement profile had an identifiable peak comprising tails proximal and distal to the cell periphery. To visualize many of these profiles simultaneously, the length of each trace was normalized such that the 20th and 80th percentile coordinates along the trace represented the locations where proximal and distal tails of the shear displacement peaks fell to 20% of the maximum, respectively (**Figure 5e**). Both shear and normal displacement profiles were normalized to the maximum shear displacement (**Figure 5f**). The mean profile for the entire dataset was generated to visualize overall trends in distribution. The mean location of the cells' edge within these profiles occurred near the center of the trace.

Interpolated Displacement Fields and Heat Maps

To visualize displacement fields measured within the hydrogels, the values of shear and normal displacement observed were interpolated using a bi-cubic interpolation scheme to generate displacement information at a pixel density equal to the resolution of the original images (6.153 pixel/μm). Interpolated data were used to determine the sum of shear or sum of normal deformations used in the analysis of shear and normal displacement relationships.

Statistical Information

All error bars and textual value ranges represent one standard deviation from the associated mean value. Linear regression models (**Figure 5**) were generated using the Matlab fitlm function, and the associated R^2, p-value, and sample size, n, are reported for each line. For some data, also reported are the x-coefficient representing the slope of the regression line.

References

(1) Cuchiara, M. L.; Horter, K. L.; Banda, O. a; West, J. L. Covalent Immobilization of Stem Cell Factor and Stromal Derived Factor 1α for in Vitro Culture of Hematopoietic Progenitor Cells. *Acta Biomater.* **2013**, *9* (12), 9258–9269. https://doi.org/10.1016/j.actbio.2013.08.012.

(2) Cruise, G. M.; Scharp, D. S.; Hubbell, J. a. Characterization of Permeability and Network Structure of Interfacially Photopolymerized Poly(Ethylene Glycol) Diacrylate Hydrogels. *Biomaterials* **1998**, *19* (14), 1287–1294.

(3) Majima, T.; Schnabel, W.; Weber, W. Phenyl-2,4,6-Trimethylbenzoylphosphinates as Water-Soluble Photoinitiators. Generation and Reactivity of O=P(C6H5)(O−) Radical Anions. *Die Makromol. Chemie* **1991**, *192* (10), 2307–2315. https://doi.org/10.1002/macp.1991.021921010.

(4) Banda, O. A. Slater Lab Git Hub Repository https://github.com/obanda310/Slater-Lab.

(5) Gao, Y.; Kilfoil, M. L. Accurate Detection and Complete Tracking of Large Populations of Features in Three Dimensions. *Opt. Express* **2009**, *17* (6), 4685. https://doi.org/10.1364/OE.17.004685.

(6) Crocker, J. C.; Grier, D. G. Methods of Digital Video Microscopy for Colloidal Studies. *J. Colloid Interface Sci.* **1996**, *179* (1), 298–310. https://doi.org/10.1006/jcis.1996.0217.

(7) http://people.umass.edu/kilfoil/downloads.html.